Supporting information

Synthesis and characterization of $M_3V_2O_8$ (M = Ni or Co) based nanostructures: a new family of high performance pseudocapacitive materials

Mao-Cheng Liu [a], Ling-Bin Kong [a,b,*], Long Kang [b], Xiaohong Li [c], Frank C. Walsh [c], Man Xing [a], Chao Lu [a], Xue-Jing Ma [a] and Yong-Chun Luo [b]

[a] *State Key Laboratory of Advanced Processing and Recycling of Nonferrous Metals, Lanzhou University of Technology, Lanzhou 730050, PR China*

[b] *School of Materials Science and Engineering, Lanzhou University of Technology, Lanzhou 730050, PR China*

[c] *Electrochemical Engineering Laboratory, Energy Technology Research Group, Faculty of Engineering and the Environment, University of Southampton, Highfield, Southampton, SO17 1BJ, United Kingdom*

* Corresponding author. Tel.: +86-931-2976579; fax: +86-931-2976578. E-mail address: konglb@lut.cn

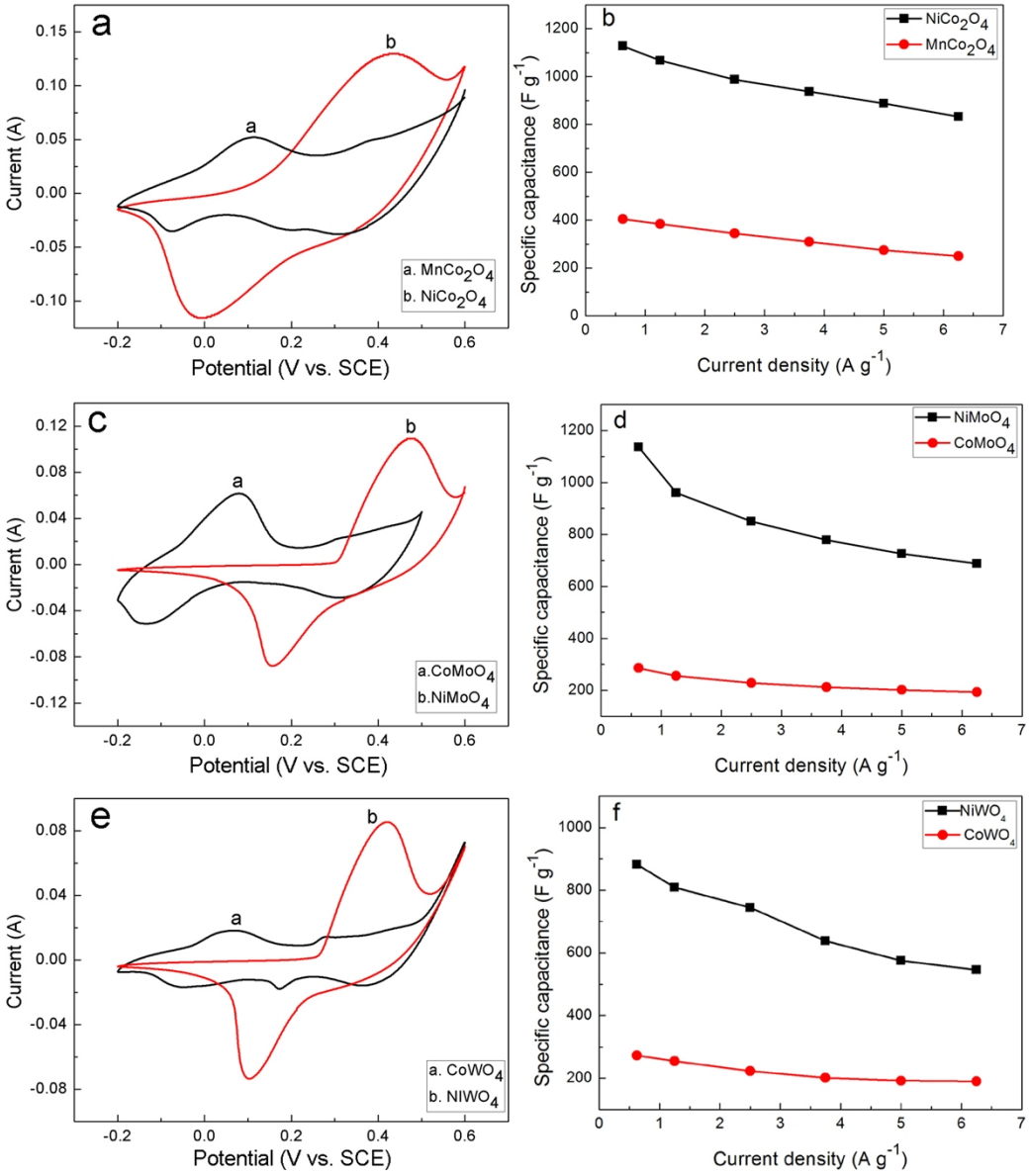

Fig. S1 (a) CV curves of $NiCo_2O_4$ and $MnCo_2O_4$ at a scan rate of 10 mV s^{-1}, (b) Specific capacitances of $NiCo_2O_4$ and $MnCo_2O_4$ at a controlled current densities. (c) CV curves of $NiMoO_4$ and $CoMoO_4$ at a scan rate of 10 mV s^{-1}, (d) Specific capacitances of $NiMoO_4$ and $CoMoO_4$ at a controlled current densities. (e) CV curves of $NiWO_4$ and $CoWO_4$ at a scan rate of 10 mV s^{-1}, (f) Specific capacitances of $NiWO_4$ and $CoWO_4$ at a controlled current densities.

Figure S1a and S1b show the CV curves and specific capacitances of the $NiCo_2O_4$ and $MnCo_2O_4$ electrodes. When the Ni was replaced by Co, the CV curve was significantly changed and their specific capacitances were greatly decreased. The CV curve of the $NiCo_2O_4$ electrode shows a pair of strong redox peaks, and the

charges associated with the anodic and cathodic peaks are almost centred on the redox peaks, while that of $MnCo_2O_4$ electrode is equably distributed in the whole scan potential window. This means that for AB_2O_4 type binary metal oxides, the A element plays important roles in the generation of pseudo capacitance. This can further be confirmed by the much higher specific capacitances of $NiCo_2O_4$ (1128, 1068, 988, 937, 888 and 833 F g^{-1} at the current densities of 0.625, 1.25, 2.5, 3.75, 5, and 6.25 A g^{-1}, respectively.) than $MnCo_2O_4$ electrodes (405, 384, 344, 309, 275 and 250 F g^{-1} at the current densities of 0.625, 1.25, 2.5, 3.75, 5, and 6.25 A g^{-1}, respectively). In order to further study the contributions of both A and B elements on pseudocapacitive properties of the ABO_4 type binary metal oxides, the CV curves and specific capacitances of the $NiMoO_4$, $CoMoO_4$, $NiWO_4$, and $CoWO_4$ electrodes are shown in Fig. S1c-S1f. In the case of both $NiMoO_4$ and $NiWO_4$, when the Ni was replaced by Co, the CV curves were significantly changed. The specific capacitances of $CoMoO_4$ (286, 256, 229, 212, 202 and 193 F g^{-1} at the current densities of 0.625, 1.25, 2.5, 3.75, 5, and 6.25 A g^{-1}, respectively.) and $CoWO_4$ (273, 254, 223, 202, 192, and 190 F g^{-1} at the current densities of 0.625, 1.25, 2.5, 3.75, 5, and 6.25 A g^{-1}, respectively.) are greatly decreased compared with $NiMoO_4$ (1136, 960, 850,778, 725, and 688 F g^{-1} at the current densities of 0.625, 1.25, 2.5, 3.75, 5, and 6.25 A g^{-1}, respectively.) and $NiWO_4$ (882, 809, 744, 638, 575, and 546 F g^{-1} at the current densities of 0.625, 1.25, 2.5, 3.75, 5, and 6.25 A g^{-1}, respectively.). This indicates that for ABO_4 binary metal oxides, the A element also plays important roles in the generation of pseudo capacitance. Besides, it can be seen that the CV curves and specific capacitances of

$NiMoO_4$ and $NiWO_4$ are close to that of $CoMoO_4$ and $CoWO_4$ electrodes, this suggest that B elements has minor influence to the capacitances of the binary metal oxides. Therefore, it is concluded that the element located in A position with lower chemical valence plays important roles in the generation of pseudocapacitance, while the B element with higher chemical valence has minor influence to the capacitances of the binary metal oxides.

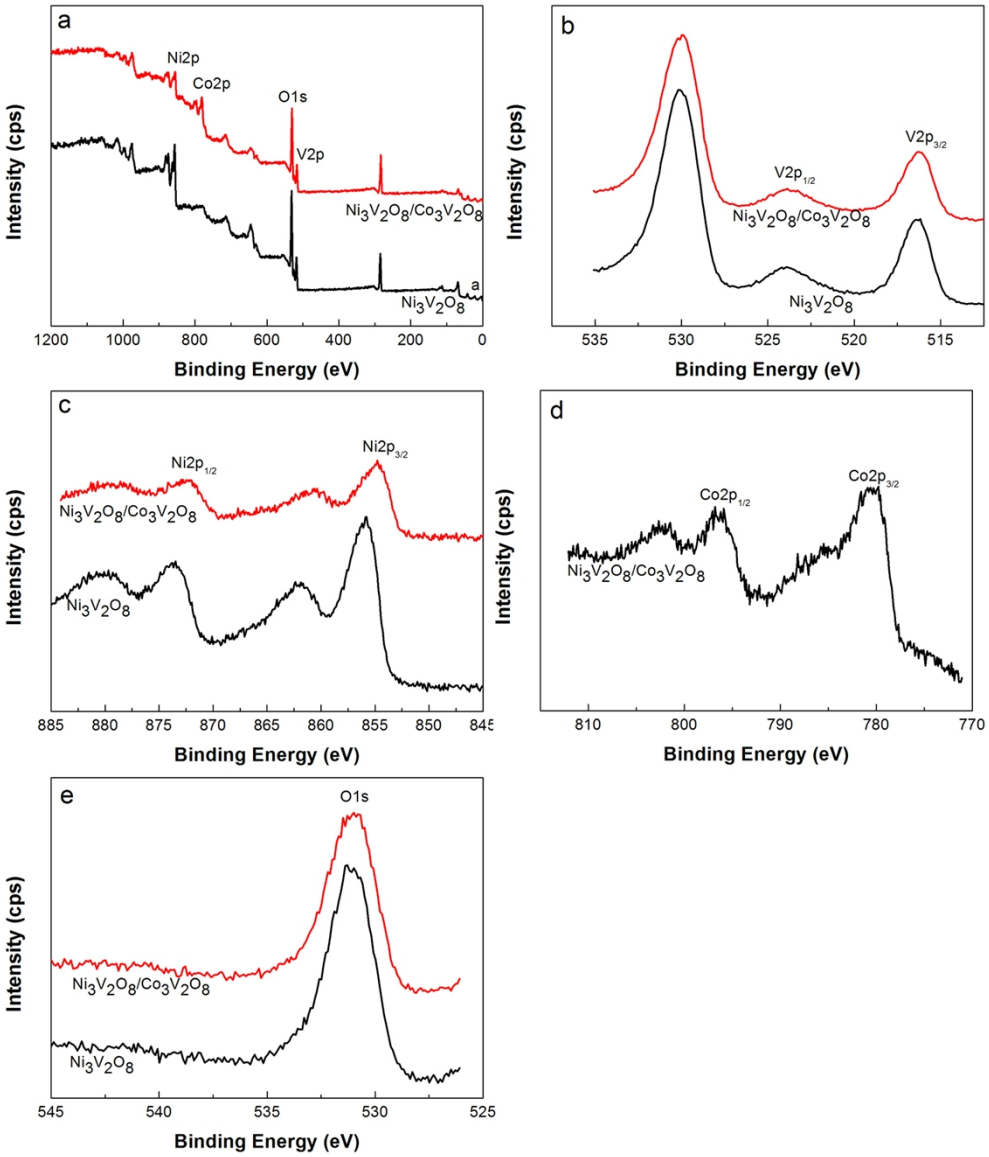

Fig. S2 (a) Overall XPS, (b) V2p, (c) Ni2p, (d) Co2p, and (e) O1s XPS spectra of the $Ni_3V_2O_8$ and $Ni_3V_2O_8/Co_3V_2O_8$ nanocomposite with a Ni/Co molar ratio of 1:1.

The overall XPS spectrum (Fig. S2a) shows the elements of the $Ni_3V_2O_8$ and $Ni_3V_2O_8/Co_3V_2O_8$ nanocomposite. The V2p corresponding to the and V^{5+}, and the Ni2p and Co2p are revealed to be Ni^{2+} and Co^{2+}, respectively. O1s XPS shows a strong peak around 530.8 eV which can be regarded as characteristic peak of O1s in $M_3V_2O_8$.

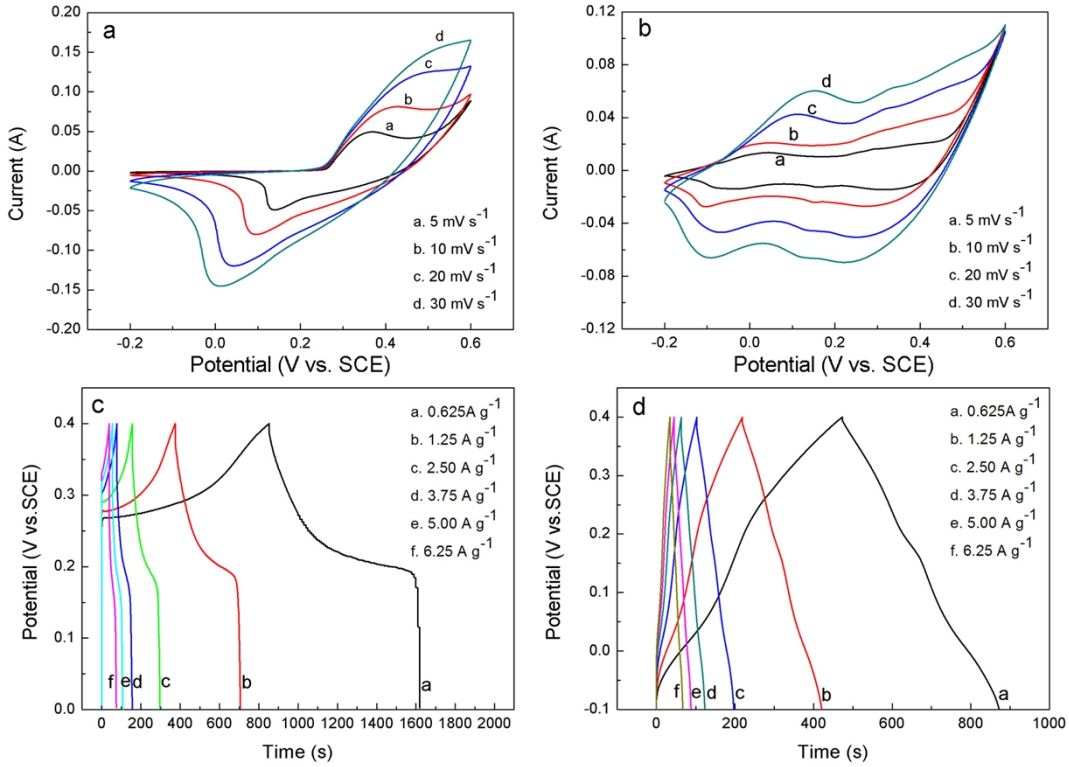

Fig.S3 Electrochemical characterizations of the $Ni_3V_2O_8$ and $Co_3V_2O_8$ electrodes. CV curves of (a) $Ni_3V_2O_8$ and (b) $Co_3V_2O_8$ electrodes at different scan rates. Charge-discharge curves of (c) $Ni_3V_2O_8$ and (d) $Co_3V_2O_8$ electrodes at controlled current densities.

Figure S3 shows the CV curves and charge-discharge curves of both $Ni_3V_2O_8$ and $Co_3V_2O_8$ electrodes. Though the CV curves of both $Ni_3V_2O_8$ and $Co_3V_2O_8$ electrodes show visible redox peaks, indicating their pseudo capacitance, the charges associated with the anodic and cathodic peaks are different. The charges of $Co_3V_2O_8$

electrode are equably distributed in the whole scan potential window, while that of $Ni_3V_2O_8$ electrode are almost centred on the redox peaks. This indicates that the faradaic reactions of $Co_3V_2O_8$ can take place in the whole potential window and will provide better rate capability, but that of $Ni_3V_2O_8$ can only occur around redox peaks and result in a poor rate capability. The shapes of the CV curves for both of the electrodes are not significantly influenced by the increase of the scan rates. This indicates the improved mass transportation and electron conduction in the host materials. The specific capacitances of the $Ni_3V_2O_8$ and $Co_3V_2O_8$ electrodes, calculated from the discharge times, are 1181, 1043, 847, 750, 692, 625 F g^{-1} and 505, 493, 470, 450, 430, 413 F g^{-1} at the discharge current densities of 0.625, 1.25, 2.5, 3.75, 5, and 6.25 A g^{-1}, respectively.

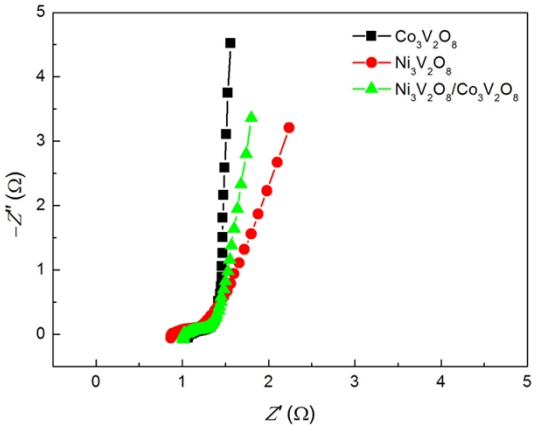

Fig.S4 Complex-plane impedance plots of $Ni_3V_2O_8$, $Co_3V_2O_8$, and $Ni_3V_2O_8/Co_3V_2O_8$ nanocomposite electrodes. The $Ni_3V_2O_8/Co_3V_2O_8$ nanocomposite has lower charge transfer resistance and ion diffusion resistance than $Ni_3V_2O_8$.

The pourbaix diagram (shown in Fig. S5) for Ni, Co and V reveals that V does not participate in any redox reaction and has no contribution to the capacitance of

$M_3V_2O_8$ (M = Ni or Co). The capacitance of $M_3V_2O_8$ is contributed by Ni and Co elements. This is in good accordance with the other reports about hierarchical $MnMoO_4/CoMoO_4$ heterostructured nanowires[1] and amorphous $NiWO_4$ nanostructure[2] as electrode materials for supercapacitors.

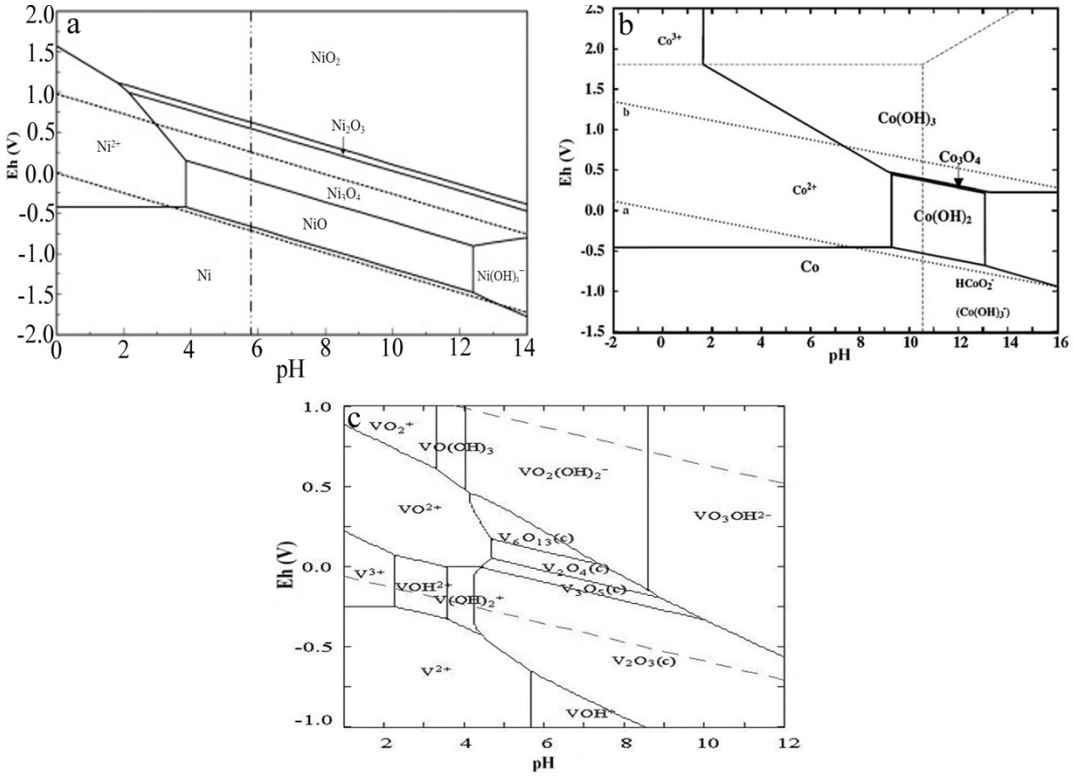

Fig.S5 Pourbaix diagram of (a) Ni, (b) Co and (c) V.

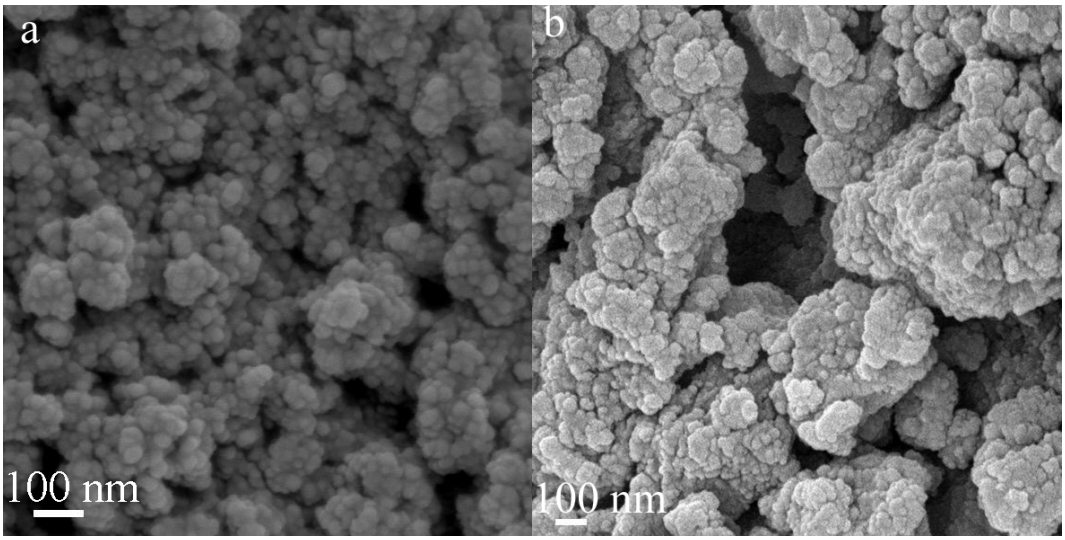

Fig.S6 SEM images (a) Before 1000 cycles and (b) after1000 cycles of the $Ni_3V_2O_8/Co_3V_2O_8$ electrodes. The microstructure and surface morphology are perfectly retained during the charge-discharge process.

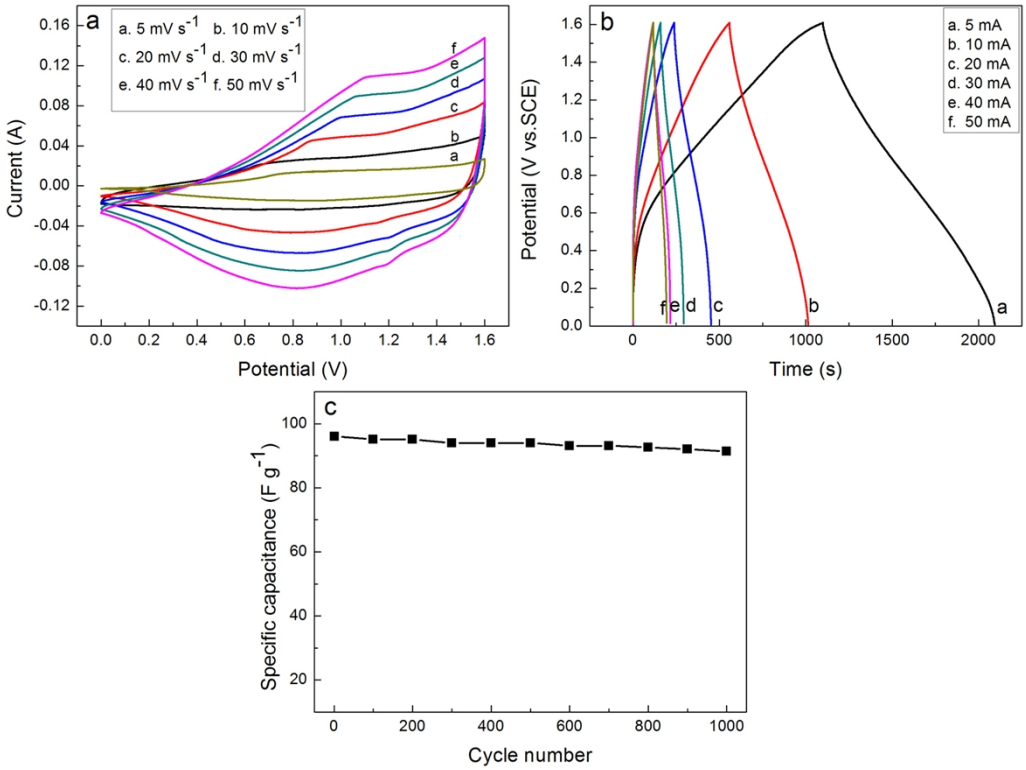

Fig. S7 (a) CV curves and (b) Charge/discharge curves of AC and $Ni_3V_2O_8/Co_3V_2O_8$ nanocomposite based asymmetric supercapacitor. (c) Cycling performance of asymmetric supercapacitor.

A two electrode configuration (asymmetric supercapacitor) in which

$Ni_3V_2O_8/Co_3V_2O_8$ nanocomposite as positive electrode and activated carbon as negative electrode is assembled to measure the capacitive performance of the $Ni_3V_2O_8/Co_3V_2O_8$ electrode. For comparison, an activated carbon based symmetric supercapacitor is also assembled. The energy density (E) and power density (P_{av}) of the supercapacitor is calculated by:

$$E = \frac{1}{2}CV^2 \quad (1)$$

$$P_{av} = \frac{E}{t} \quad (2)$$

where t represent the discharge times, C and V represent the specific capacitance and the cell voltage of the supercapacitor, respectively. In asymmetric supercapacitor, the mass balancing between positive electrode (m_+) and negative electrode (m_-) follows the Equation:

$$\frac{m_+}{m_-} = \frac{C_- \times \Delta E_-}{C_+ \times \Delta E_+} \quad (3)$$

The specific capacitance of the activated carbon and $Ni_3V_2O_8/Co_3V_2O_8$ are 187 and 1278 F g^{-1}. On the basis of potential windows found for the activated carbon and $Ni_3V_2O_8/Co_3V_2O_8$ electrodes, the mass of the activated carbon and $Ni_3V_2O_8/Co_3V_2O_8$ electrodes are 21.8 and 8 mg, respectively. After 1000 cycles, 95.2 % of the initial specific capacitance is remained.

References

1 L. Q. Mai, F. Yang, Y. L. Zhao, X. Xu, L. Xu and Y. Z. Luo, *Nat. Commun*., 2011, **2**, 381.

2 L. Y. Niu, Z. P. Li, Y. Xu, J. F. Sun, W. Hong, X. H. Liu, J. Q. Wang, and S. R. Yang, *ACS Appl. Mater. Interfaces*, 2013, **5**, 8044.